Dalton Transactions

COMMUNICATION

View Article Online
View Journal | View Issue

Cite this: *Dalton Trans.*, 2018, **47**, 35

Received 26th September 2017,
Accepted 13th November 2017

DOI: 10.1039/c7dt03623j

rsc.li/dalton

A spin crossover (SCO) active graphene-iron(II) complex hybrid material†

Kuppusamy Senthil Kumar, *[a] Ivan Šalitroš,[b] Zahia Boubegtiten-Fezoua,[c] Simona Moldovan,[a,d] Petra Hellwig [c] and Mario Ruben *[a,e]

The advancement of molecular electronics and spintronics requires novel hybrid materials with synergistic magnetic and electrical properties. The non-covalent functionalization of highly conductive graphene with magnetically bistable spin crossover (SCO) complexes may yield such a multifunctional material. In this regard, a graphene-Fe(II) SCO complex hybrid (Gr-SCO) has been prepared by non-covalently anchoring a pyrene decorated SCO complex with solution phase pre-exfoliated few-layer graphene sheets. SQUID magnetometry revealed the preservation of SCO in the Gr-SCO hybrid material exhibiting more gradual spin state switching characteristics than in the bulk molecular complex. This persistence of SCO of a molecular Fe(II) complex upon anchoring on the graphene surface has consequences towards the realization of SCO based applications: in (i) reversible spin state dependent band gap tuning of graphene with an SCO complex analogous to chemical doping of graphene, and (ii) to probe the spin state dependence of electrical conductivity modulation by wiring the anchoring group (pyrene) tethered SCO complex between chemically robust few-layer graphene electrodes.

Graphene is a highly studied 2D material due to its attractive electrical and mechanical properties that are promising for applications in electronics, spintronics, and nanomechanics.[1–4] Graphene can be manipulated by external means; this opens the possibility to exploit interfacial proximity effects and functionalization.[5,6] For instance, graphene metal interface or molecular functionalization has been reported to induce superconductivity, insulating behavior, or magnetic properties.[7–11] Graphene or respective few-layer graphene is also utilized as an electrode for single molecule conductance measurements due to their thermostability down to few Kelvins (K).[12–15] Spin crossover (SCO) has been observed in metal–organic molecules featuring first-row transition metal ions with d^4–d^7 electronic configuration in a moderate ligand field.[16–28] The room temperature (RT) low spin (LS) → high spin (HS) bistability of the Fe(II) SCO complexes,[20,21] effected by temperature, light, pressure, electric field, and mechanical stretching,[29–38] augurs well for the realization of SCO based applications.[16,19–21,39] Further, computational and experimental results detailing spin-state dependent electrical conductivity modulations and spin filtering effects in SCO-molecular junctions render the SCO systems suitable for the fabrication of molecular electronics/spintronics device architectures.[37,40–43] In this context, the marriage between an SCO active entity and graphene may yield a synergistic graphene-SCO hybrid (Gr-SCO) with alluring magnetic and electrical characteristics. Graphene could also be employed as a weekly interacting surface to preserve switching characteristics of SCO active entities in view of the reports detailing surface-induced suppression/blocking of SCO due to strong interfacial molecule–surface interactions.[44–51] Studies detailing (i) preservation of SCO of molecular and polymeric adsorbates on highly oriented pyrolytic graphite (HOPG)[52] and graphene[53] substrates, (ii) spin state dependent electrical conductivity modulations in graphene or reduced graphene oxide (rGO) substrates functionalized with SCO active entities,[54] and (iii) utility of graphene substrate as an analytical probe to study SCO in NP thin films,[55] have appeared in the recent literature clearly elucidating the application potential of

[a]*Institut de Physique et Chimie des Matériaux de Strasbourg (IPCMS), CNRS-Université de Strasbourg, 23, rue du Loess, BP 43, 67034 Strasbourg cedex 2, France. E-mail: senthil.kuppusamy@ipcms.unistra.fr*

[b]*Institute of Inorganic Chemistry, Technology and Materials, Faculty of Chemical and Food Technology, Slovak University of Technology, Bratislava, 81237, Slovak Republic*

[c]*Laboratoire de Bioélectrochimie et Spectroscopie, UMR 7140, Chimie de la Matière Complexe, Université de Strasbourg CNRS, 1, rue Blaise Pascal, 67081 Strasbourg, France*

[d]*Groupe de Physique des Matériaux (GPM), UMR 6634, CNRS–Université de Normandie–INSA de Rouen, Avenue de l'Université – BP12, 76801 Saint Etienne du Rouvray, France*

[e]*Institute of Nanotechnology, Karlsruhe Institute of Technology (KIT), Hermann-von-Helmholtz-Platz 1, 76344 Eggenstein-Leopoldshafen, Germany. E-mail: mario.ruben@kit.edu*

†Electronic supplementary information (ESI) available: Experimental details related to magnetic and variable temperature infrared (VT-IR) measurements. Plots of thermal and photomagnetic, Raman, ATR-IR, and VT-FIR characteristics of ligand, complex **1** and graphene-SCO hybrid. See DOI: 10.1039/c7dt03623j

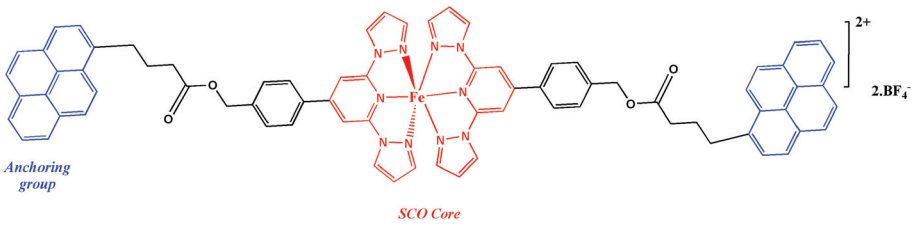

Fig. 1 Molecular structure of the SCO complex, hereafter complex **1**, tethered with pyrene anchoring groups for non-covalent functionalization of graphene.

Gr-SCO hybrids. However, switching characteristics of a supramolecular Fe(II) SCO complex,[56,57] which is non-covalently anchored on a graphene surface are to be reported. Probing in this direction may facilitate an understanding of the role of graphene proximity in altering SCO characteristics necessary to build Gr-SCO based molecular electronics/spintronics devices. To begin with, a pyrene anchoring group tethered bis(pyrazol-1-yl)pyridine (BPP)-Fe(II) SCO active complex[56] (*cf.* Fig. 1) is utilized to prepare a Gr-SCO hybrid material taking advantage of the noncovalent π–π interactions between pyrene and graphene surface. Temperature and light induced variations of the magnetic properties between the molecular SCO complex **1** and Gr-SCO hybrid are detailed as follows.

The Gr-SCO hybrid material was obtained by non-covalently anchoring the complex **1** on the pre-exfoliated graphene sheets with the aid of the pyrene anchoring groups. Attempts to get Gr-SCO hybrid directly from exfoliation of the bulk graphite using complex **1** were not successful, partly attributed to the unstable nature of the complex **1** under rigorous sonication conditions. To alleviate this problem, a novel strategy has been developed utilizing commercially available graphene sheet dispersions in water. By repeated precipitation, re-dispersion and centrifugation, dispersions of graphene sheets in 1,2-dichloroethane (1,2-DCE) were obtained. Gr-SCO hybrid materials were finally prepared by mixing the acetonitrile solution of the complex **1** with the preformed graphene dispersion and precipitation of the hybrid by layering diethyl ether over a period of 1–2 weeks as depicted in Fig. 2.

To check for reproducibility, a set of Gr-SCO hybrids, Gr-SCO-A and Gr-SCO-B, has been prepared employing the same experimental conditions. The sample Gr-SCO-A was utilized to perform transmission electron microscopy (TEM), Infrared (IR), and Raman characterization experiments while SCO characteristics of both samples, Gr-SCO-A and Gr-SCO-B, were probed using SQUID magnetometry to check the reproducibility of the results.

The TEM analysis of the Gr-SCO-A hybrid material showed the presence of few-layer graphene sheets and locally the occurrence of single graphene layers as shown in Fig. 3a. The *Z*-contrast achieved in the high angular annular detection (HAADF) mode within the scanning transmission electron microscopy (STEM) confirmed the presence of the complex **1** on the graphene sheets as small aggregates (*cf.* Fig. 3b, inset). The elemental maps acquired in these regions revealed the

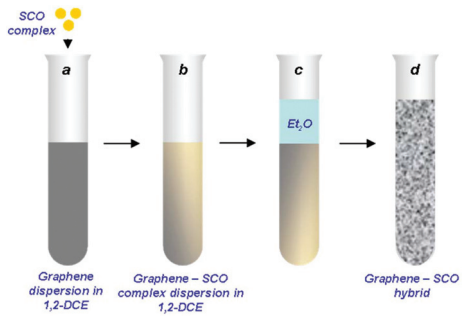

Fig. 2 Steps involved in the preparation of Gr-SCO complex hybrid: (a) complex **1** was dispersed in pre-exfoliated graphene sheets in 1,2-DCE, (b) the dispersion was centrifuged at 500 rpm for 30 min followed by removal of ~3/4th of the supernatant, (c) layering of diethyl ether over the supernatant solution, and (d) precipitation of the Gr-SCO hybrid. Filtration of the slurry over a PTFE membrane, washing with cold 1 : 1 1,2-DCE/acetonitrile solvent mixture followed by drying under vacuum yielded the Gr-SCO hybrids as black powder.

peaks corresponding to Fe thus confirming the successful anchoring of aggregates of complex **1** on the graphene sheets.

Raman spectral analysis of the Gr-SCO-A hybrid further confirms the presence of single/few-layer graphene sheets. The characteristic D, G, and 2D bands were observed in the Raman spectrum of Gr-SCO-A hybrid at the expected frequencies as shown in Fig. 4a. The strong D and D′ bands centered at 1350 and 1620 cm^{-1} originate from the small nanometer (nm) sized graphene/few-layer graphene sheets with defective edges contributing to the occurrence of the double resonant Raman effect,[58,59] which increase at lower lateral dimensions. The defective sheets are likely to happen during ultrasound treatment as also observed in the case of a porphyrin-graphene hybrid.[60]

The 2D peak can be fitted with a single Lorentzian with a full width at half maximum (FWHM) of 59 cm^{-1} implying very weak interlayer coupling and non-ABAB stacking. This could be attributed to the random bundling/aggregation of graphene sheets in line with the literature reports.[61] The Raman features of the complex **1** in the Gr-SCO-A hybrid are masked by the intense peaks corresponding to the graphene substrate (Fig. 4a). See Fig. S1† for the Raman spectra of ligand and the complex **1** showing similar spectral profiles thus confirming the identity of the ligand skeleton in the complex **1**.

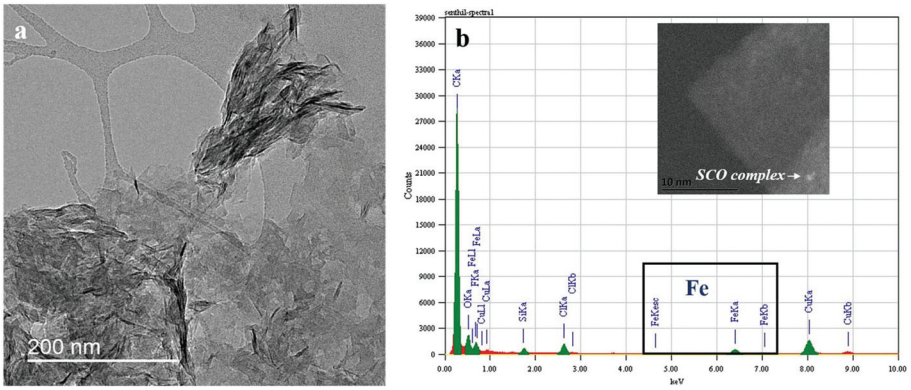

Fig. 3 (a) TEM micrograph of Gr-SCO-A hybrid material and (b) EDX profile of the hybrid, the inset shows the corresponding HAADF-STEM image of small crystallites of the complex **1** on graphene surface.

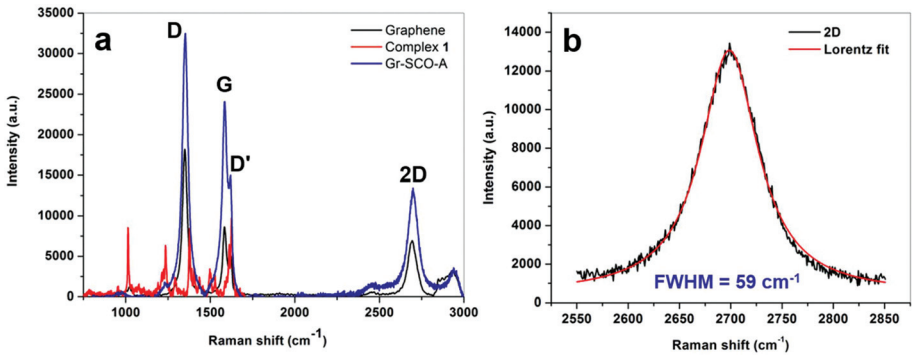

Fig. 4 (a) Raman spectra of graphene, complex **1** (see Fig. S1† for full spectrum), and Gr-SCO-A hybrid and (b) single Lorentz function fitted 2D band corresponding to graphene in Gr-SCO-A with an FWHM of 59 cm^{-1}. The excitation laser wavelength (λ) is 514 nm.

Attenuated total reflection-infrared (ATR-IR) spectroscopic studies of the ligand, complex **1**, and Gr-SCO-A hybrid samples on a diamond crystal at 294 K and the comparisons of the spectral features among them showed the presence of the complex **1** on graphene. See Fig. S2† and Table S1 for further details.

Variable temperature magnetic investigations have been performed on two independently prepared Gr-SCO hybrid material samples, denoted in the following as Gr-SCO-A and Gr-SCO-B (Fig. 5).

In both cases, a gradual increase of the magnetic moment above 100 K is observed, which is undoubtedly a signature of SCO. Unlike the polycrystalline complex **1** (Fig. 5), thermally induced SCO of hybrid materials will reach HS plateau above 300 K. Such loss of abruptness in SCO curve is explained by the significant decrease of cooperativity caused by dilution, *i.e.*, lack of intermolecular interactions, of complex **1** on the graphene surface. The magnetic characteristics of the Gr-SCO hybrids are not probed below 50 K due to the paramagnetic nature (*cf.* Fig. S3†) of the graphene sheets utilized in this study, *vide infra*.

The observed $T_{1/2}$ values of 232 and 242 K for Gr-SCO-A and Gr-SCO-B, respectively are higher than the $T_{1/2}$ = 220 K found for polycrystalline complex **1**. This can be attributed to the strong interfacial interactions between the SCO complex and 2D graphene lattice hindering the occurrence of the SCO

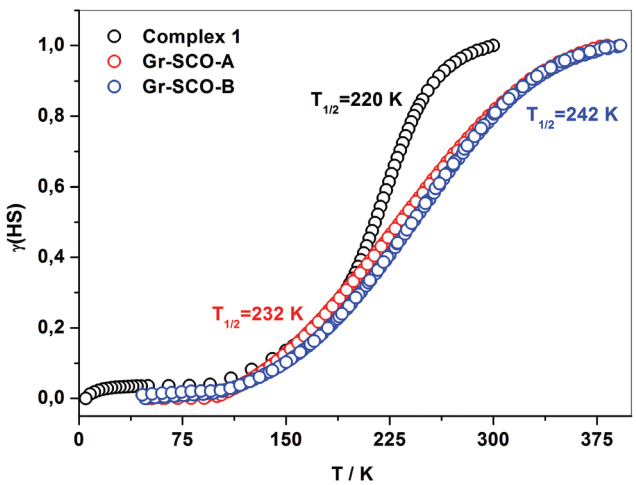

Fig. 5 SCO characteristics of complex **1** and hybrid samples Gr-SCO-A and Gr-SCO-B.

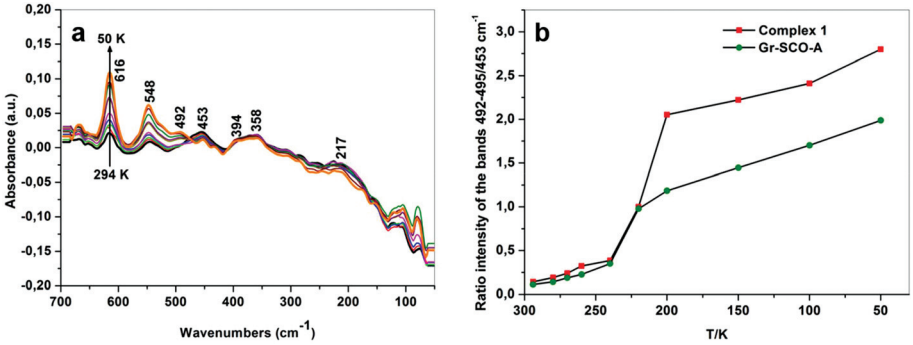

Fig. 6 (a) VT-FIR spectra of Gr-SCO-A hybrid in the temperature range of 294 to 50 K and (b) intensity ratio *vs.* *T* plots of complex **1** and Gr-SCO-A hybrid. The intensity ratio of the bands, 495/453 and 492/453 cm^{-1} have been considered for complex **1** and Gr-SCO-A, respectively.

event, a facet conceptually related to the lattice dilution effects affecting SCO characteristics of Fe(II) complexes dispersed in solid matrices comprised of transition metal ions either larger or smaller in radius relative to the Fe(II) ion.[62]

Though the samples Gr-SCO-A and Gr-SCO-B have shown slightly different SCO characteristics, the methodology employed to prepare Gr-SCO hybrids are satisfactorily reproducible as inferred from the atomic absorption spectroscopy (AAS) analysis of the hybrid materials. The Iron content of the samples Gr-SCO-A and Gr-SCO-B are found to be 1.81% and 2.09%, respectively indicating the quantitatively comparable amount of complex **1** molecules anchored on the graphene surface. Hence, the variations in the SCO characteristics of Gr-SCO-A and Gr-SCO-B are attributed to the slightly differing local interactions between the graphene and complex **1** as reported in the case of supramolecular spin valve devices comprised of single-walled carbon nanotube (SWNT) and a single molecule magnet (SMM). The supramolecular SWNT-SMM devices have shown different magneto-conductance behavior as a result of slight local variations of the coupling between the SMMs and the SWNTs.[63]

Photomagnetic studies revealed light induced excited spin state trapping (LIESST) of complex **1** with quantitative LS → HS photoconversion (*cf.* Fig. S4†) upon red light irradiation (λ = 637 nm; 10 mW cm^{-2}) with a photoexcited metastable HS state stable up to 76 K (T_{LIESST}). The Gr-SCO-A hybrid is also LIESST active and at 10 K exhibiting photoconversion to the HS state upon irradiation at 637 nm (Fig. S5†), with T_{LIESST} = *ca.* 60 K, which is in agreement with "inverse energy gap" theory relating thermal SCO with LIESST.[64] The exact quantification of the photoinduced SCO characteristics of Gr-SCO-A is found to be difficult due to a small quantity of complex **1** anchored on the graphene surface.

Variable temperature far-infrared (VT-FIR) spectroscopic investigations of complex **1** and Gr-SCO-A hybrid further confirmed the spin-state switching characteristics of the hybrid in line with the SQUID magnetometry. VT-FIR experiments of the complex **1** in the 294–50 K range showed a clear decrease and increase in the intensity of bands at 453 cm^{-1} and 495 cm^{-1}, respectively (*cf.* Fig. S6†). Similar trends were observed for the Gr-SCO-A hybrid (Fig. 6a) except for a slight down shifting of the higher energy band to 492 cm^{-1} (495 cm^{-1} for complex **1**). Any effect on the complex **1** structure in the Gr-SCO-A hybrid by the vacuum has been excluded.

This higher intensity of the bands (495 or 492 cm^{-1}) upon temperature reduction from 294 to 50 K could be tentatively attributed to the HS → LS transition of complex **1** and Gr-SCO-A. In addition to the spin transition, a linear increase of the overall intensity, typical for far infrared spectra is identified for several signals between 650 and 450 cm^{-1}. This is characteristic for glass-like transitions of complex compounds due to increased interactions at low temperatures.[60] The plot of the ratio of intensities for complex **1** and Gr-SCO-A (Fig. 6b) are in line with the SQUID magnetometry indicating more gradual SCO characteristics of Gr-SCO-A in comparison with complex **1**. Though the above VT-FIR experiments are in close agreement with the SQUID magnetometry, the results should be treated with caution; particularly the assignment of LS and HS features corresponding to the Fe-BPP complex system. The HS state of the Fe-BPP complexes is reported to show ν(Fe–N) vibrations at 247, 255, and 303 cm^{-1},[65] finding those bands in the complex **1** and Gr-SCO-A hybrid is proved to be difficult due to several overlapping skeletal vibrations belonging to the ligand backbone (*cf.* Fig. S7†). Note also the difficulties reported in the literature associated with the finding of LS vibrations located around 400 cm^{-1} due to masking of ligand centered skeletal vibrations.[65,66] The absence of reversible temperature-dependent intensity variation of the bands around 453 and 495 cm^{-1} for the ligand in the VT-FIR experiments (*cf.* Fig. S7†) is a clear proof of spin-state switching mediated evolution of the VT-FIR characteristics of Gr-SCO-A in line with the SQUID measurements.

Though the hybrids Gr-SCO-A and Gr-SCO-B show more gradual switching characteristics, relative to the molecular complex, their magnetic moment *vs.* *T* plot is markedly different leading to the observation of two different $T_{1/2}$ values indicating slightly different intermolecular and molecule–graphene interactions in Gr-SCO-A and Gr-SCO-B hybrids. The results obtained in this study also need to be discussed by taking into consideration the magnetic properties associated

with nano-graphene materials.[67] The presence of lattice defects and edge states in graphene/few-layer graphene sheets contributes to the observation of various exotic magnetic phenomena, see a perspective article by Rao *et al.*, for further information on this topic.[67] By analogy with the literature report, the magnetic moment *vs.* *T* plot of the graphene sample utilized in this study showed paramagnetic behaviour below 50 K (*cf.* Fig. S3†) which can be attributed to the defect induced magnetism of graphene in line with the literature reports, also note afore-described Raman spectral studies showing defective nature of the graphene sheets. However, the SCO characteristics of Gr-SCO-A and Gr-SCO-B reported in this study unambiguously originate from the complex **1** anchored on the graphene surface, the diamagnetic nature of the graphene sample above ~50 K is a conclusive proof of this attribution.

In summary, Gr-SCO hybrids, Gr-SCO-A and Gr-SCO-B, comprising of pre-exfoliated graphene sheets and an SCO active complex **1**, are prepared, and their SCO characteristics have been studied. The hybrids retained SCO with alterations in SCO characteristics attributed to the 2D graphene proximity mediated interfacial and matrix dilution effects. Issues such as reproducibility of switching characteristics of Gr-SCO hybrids and inherent magnetism associated with defective graphene sheets utilized to prepare Gr-SCO hybrids have also been addressed. The results presented in this study might be useful for the development of SCO-based spintronic applications.

Conflicts of interest

There are no conflicts of interest to declare.

Acknowledgements

Grant Agencies (France: Innovation FRC: Self-assembly of spin crossover (SCO) complexes on graphene; Germany: Deutsche Forschungsgemeinschaft (DFG) through TRR 88 "3MET" (C5), Slovakia: APVV-14-0078, APVV-14-0073, VEGA 1/0522/14, STU Grant scheme for Support of Excellent Teams of Young Researchers and COST Action CM1305 (ECOSTBio) are acknowledged for the financial support. We are also indebted to the icFRC (Strasbourg) for continuous support).

References

1 K. S. Novoselov, *Science*, 2004, **306**, 666–669.
2 W. Han, R. K. Kawakami, M. Gmitra and J. Fabian, *Nat. Nanotechnol.*, 2014, **9**, 794–807.
3 C. Chen, S. Rosenblatt, K. I. Bolotin, W. Kalb, P. Kim, I. Kymissis, H. L. Stormer, T. F. Heinz and J. Hone, *Nat. Nanotechnol.*, 2009, **4**, 861–867.
4 K. S. Novoselov, A. K. Geim, S. V. Morozov, D. Jiang, M. I. Katsnelson, I. V. Grigorieva, S. V. Dubonos and A. A. Firsov, *Nature*, 2005, **438**, 197–200.
5 V. Georgakilas, M. Otyepka, A. B. Bourlinos, V. Chandra, N. Kim, K. C. Kemp, P. Hobza, R. Zboril and K. S. Kim, *Chem. Rev.*, 2012, **112**, 6156–6214.
6 Y. Xu, H. Bai, G. Lu, C. Li and G. Shi, *J. Am. Chem. Soc.*, 2008, **130**, 5856–5857.
7 B. M. Kessler, Ç. Ö. Girit, A. Zettl and V. Bouchiat, *Phys. Rev. Lett.*, 2010, **104**, 047001.
8 H. B. Heersche, P. Jarillo-Herrero, J. B. Oostinga, L. M. K. Vandersypen and A. F. Morpurgo, *Nature*, 2007, **446**, 56–59.
9 D. C. Elias, R. R. Nair, T. M. G. Mohiuddin, S. V. Morozov, P. Blake, M. P. Halsall, A. C. Ferrari, D. W. Boukhvalov, M. I. Katsnelson, A. K. Geim and K. S. Novoselov, *Science*, 2009, **323**, 610–613.
10 A. V. Krasheninnikov, P. O. Lehtinen, A. S. Foster, P. Pyykkö and R. M. Nieminen, *Phys. Rev. Lett.*, 2009, **102**, 126807.
11 Y. S. Dedkov, M. Fonin, U. Rüdiger and C. Laubschat, *Phys. Rev. Lett.*, 2008, **100**, 107602.
12 F. Prins, A. Barreiro, J. W. Ruitenberg, J. S. Seldenthuis, N. Aliaga-Alcalde, L. M. K. Vandersypen and H. S. J. van der Zant, *Nano Lett.*, 2011, **11**, 4607–4611.
13 E. Burzurí, J. O. Island, R. Díaz-Torres, A. Fursina, A. González-Campo, O. Roubeau, S. J. Teat, N. Aliaga-Alcalde, E. Ruiz and H. S. J. van der Zant, *ACS Nano*, 2016, **10**, 2521–2527.
14 H. Sadeghi, S. Sangtarash and C. Lambert, *Nano Lett.*, 2017, **17**, 4611–4618.
15 S. Lumetti, A. Candini, C. Godfrin, F. Balestro, W. Wernsdorfer, S. Klyatskaya, M. Ruben and M. Affronte, *Dalton Trans.*, 2016, **45**, 16570–16574.
16 *Spin-crossover materials: properties and applications*, ed. M. A. Halcrow, John Wiley & Sons Ltd, Oxford, UK, 2013.
17 P. N. Martinho, C. Rajnak and M. Ruben, in *Spin-Crossover Materials*, ed. M. A. Halcrow, John Wiley & Sons Ltd, Oxford, UK, 2013, pp. 375–404.
18 K. S. Kumar and M. Ruben, *Coord. Chem. Rev.*, 2017, **346**, 176–205.
19 K. S. Kumar, I. Šalitroš, B. Heinrich, O. Fuhr and M. Ruben, *J. Mater. Chem. C*, 2015, **3**, 11635–11644.
20 I. Šalitroš, N. T. Madhu, R. Boča, J. Pavlik and M. Ruben, *Monatsh. Chem.*, 2009, **140**, 695–733.
21 B. Schäfer, C. Rajnák, I. Šalitroš, O. Fuhr, D. Klar, C. Schmitz-Antoniak, E. Weschke, H. Wende and M. Ruben, *Chem. Commun.*, 2013, **49**, 10986.
22 E. J. Devid, P. N. Martinho, M. V. Kamalakar, I. Šalitroš, Ú. Prendergast, J.-F. Dayen, V. Meded, T. Lemma, R. González-Prieto, F. Evers, T. E. Keyes, M. Ruben, B. Doudin and S. J. van der Molen, *ACS Nano*, 2015, **9**, 4496–4507.
23 B. Weber, W. Bauer and J. Obel, *Angew. Chem., Int. Ed.*, 2008, **47**, 10098–10101.

24 G. Molnár, L. Salmon, W. Nicolazzi, F. Terki and A. Bousseksou, *J. Mater. Chem. C*, 2014, **2**, 1360–1366.
25 S. Hayami, S. M. Holmes and M. A. Halcrow, *J. Mater. Chem. C*, 2015, **3**, 7775–7778.
26 A. Bousseksou, G. Molnár, L. Salmon and W. Nicolazzi, *Chem. Soc. Rev.*, 2011, **40**, 3313.
27 S. Brooker, *Chem. Soc. Rev.*, 2015, **44**, 2880–2892.
28 E. Breuning, M. Ruben, J.-M. Lehn, F. Renz, Y. Garcia, V. Ksenofontov, P. Gütlich, E. Wegelius and K. Rissanen, *Angew. Chem., Int. Ed.*, 2000, **39**, 2504–2507.
29 E. A. Osorio, K. Moth-Poulsen, H. S. J. van der Zant, J. Paaske, P. Hedegård, K. Flensberg, J. Bendix and T. Bjørnholm, *Nano Lett.*, 2010, **10**, 105–110.
30 V. Meded, A. Bagrets, K. Fink, R. Chandrasekar, M. Ruben, F. Evers, A. Bernand-Mantel, J. S. Seldenthuis, A. Beukman and H. S. J. van der Zant, *Phys. Rev. B: Condens. Matter*, 2011, **83**, 245415.
31 T. G. Gopakumar, F. Matino, H. Naggert, A. Bannwarth, F. Tuczek and R. Berndt, *Angew. Chem., Int. Ed.*, 2012, **51**, 6262–6266.
32 G. D. Harzmann, R. Frisenda, H. S. J. van der Zant and M. Mayor, *Angew. Chem., Int. Ed.*, 2015, **54**, 13425–13430.
33 R. Frisenda, G. D. Harzmann, J. A. Celis Gil, J. M. Thijssen, M. Mayor and H. S. J. van der Zant, *Nano Lett.*, 2016, **16**, 4733–4737.
34 N. Baadji, M. Piacenza, T. Tugsuz, F. D. Sala, G. Maruccio and S. Sanvito, *Nat. Mater.*, 2009, **8**, 813–817.
35 T. Miyamachi, M. Gruber, V. Davesne, M. Bowen, S. Boukari, L. Joly, F. Scheurer, G. Rogez, T. K. Yamada, P. Ohresser, E. Beaurepaire and W. Wulfhekel, *Nat. Commun.*, 2012, **3**, 938.
36 S. Sanvito, *Chem. Soc. Rev.*, 2011, **40**, 3336.
37 D. Aravena and E. Ruiz, *J. Am. Chem. Soc.*, 2012, **134**, 777–779.
38 M. Chattopadhyaya, M. M. Alam and S. Chakrabarti, *RSC Adv.*, 2013, **3**, 19894.
39 *Spin crossover in transition metal compounds*, ed. P. Gütlich and H. A. Goodwin, Springer, Berlin, New York, 2004.
40 S. A. Tawfik, L. Weston, X. Y. Cui, S. P. Ringer and C. Stampfl, *J. Phys. Chem. Lett.*, 2017, **8**, 2189–2194.
41 A. Rotaru, J. Dugay, R. P. Tan, I. A. Guralskiy, L. Salmon, P. Demont, J. Carrey, G. Molnár, M. Respaud and A. Bousseksou, *Adv. Mater.*, 2013, **25**, 1745–1749.
42 C. Lefter, V. Davesne, L. Salmon, G. Molnár, P. Demont, A. Rotaru and A. Bousseksou, *Magnetochemistry*, 2016, **2**, 18.
43 E. Ruiz, *Phys. Chem. Chem. Phys.*, 2014, **16**, 14–22.
44 B. Warner, J. C. Oberg, T. G. Gill, F. El Hallak, C. F. Hirjibehedin, M. Serri, S. Heutz, M.-A. Arrio, P. Sainctavit, M. Mannini, G. Poneti, R. Sessoli and P. Rosa, *J. Phys. Chem. Lett.*, 2013, **4**, 1546–1552.
45 T. G. Gopakumar, M. Bernien, H. Naggert, F. Matino, C. F. Hermanns, A. Bannwarth, S. Mühlenberend, A. Krüger, D. Krüger, F. Nickel, W. Walter, R. Berndt, W. Kuch and F. Tuczek, *Chem. – Eur. J.*, 2013, **19**, 15702–15709.
46 A. Pronschinske, R. C. Bruce, G. Lewis, Y. Chen, A. Calzolari, M. Buongiorno-Nardelli, D. A. Shultz, W. You and D. B. Dougherty, *Chem. Commun.*, 2013, **49**, 10446.
47 S. Ossinger, H. Naggert, L. Kipgen, T. Jasper-Toennies, A. Rai, J. Rudnik, F. Nickel, L. M. Arruda, M. Bernien, W. Kuch, R. Berndt and F. Tuczek, *J. Phys. Chem. C*, 2017, **121**, 1210–1219.
48 V. Shalabaeva, S. Rat, M. D. Manrique-Juarez, A.-C. Bas, L. Vendier, L. Salmon, G. Molnár and A. Bousseksou, *J. Mater. Chem. C*, 2017, **5**, 4419–4425.
49 T. Jasper-Tönnies, M. Gruber, S. Karan, H. Jacob, F. Tuczek and R. Berndt, *J. Phys. Chem. Lett.*, 2017, **8**, 1569–1573.
50 S. Beniwal, X. Zhang, S. Mu, A. Naim, P. Rosa, G. Chastanet, J.-F. Létard, J. Liu, G. E. Sterbinsky, D. A. Arena, P. A. Dowben and A. Enders, *J. Phys.: Condens. Matter*, 2016, **28**, 206002.
51 A. Pronschinske, Y. Chen, G. F. Lewis, D. A. Shultz, A. Calzolari, M. Buongiorno Nardelli and D. B. Dougherty, *Nano Lett.*, 2013, **13**, 1429–1434.
52 M. Bernien, H. Naggert, L. M. Arruda, L. Kipgen, F. Nickel, J. Miguel, C. F. Hermanns, A. Krüger, D. Krüger, E. Schierle, E. Weschke, F. Tuczek and W. Kuch, *ACS Nano*, 2015, **9**, 8960–8966.
53 D. Qiu, D.-H. Ren, L. Gu, X.-L. Sun, T.-T. Qu, Z.-G. Gu and Z. Li, *RSC Adv.*, 2014, **4**, 31323.
54 S. Hayami, Z. Gu, H. Yoshiki, A. Fujishima and O. Sato, *J. Am. Chem. Soc.*, 2001, **123**, 11644–11650.
55 J. Dugay, M. Aarts, M. Giménez-Marqués, T. Kozlova, H. W. Zandbergen, E. Coronado and H. S. J. van der Zant, *Nano Lett.*, 2017, **17**, 186–193.
56 R. González-Prieto, B. Fleury, F. Schramm, G. Zoppellaro, R. Chandrasekar, O. Fuhr, S. Lebedkin, M. Kappes and M. Ruben, *Dalton Trans.*, 2011, **40**, 7564.
57 K. S. Kumar, I. Šalitroš, E. Moreno-Pineda and M. Ruben, *Dalton Trans.*, 2017, **46**, 9765–9768.
58 L. M. Malard, M. A. Pimenta, G. Dresselhaus and M. S. Dresselhaus, *Phys. Rep.*, 2009, **473**, 51–87.
59 P. Venezuela, M. Lazzeri and F. Mauri, *Phys. Rev. B: Condens. Matter*, 2011, **84**, 035433.
60 J. Malig, A. W. I. Stephenson, P. Wagner, G. G. Wallace, D. L. Officer and D. M. Guldi, *Chem. Commun.*, 2012, **48**, 8745.
61 A. A. Green and M. C. Hersam, *Nano Lett.*, 2009, **9**, 4031–4036.
62 P. Ganguli, P. Guetlich and E. W. Mueller, *Inorg. Chem.*, 1982, **21**, 3429–3433.
63 M. Urdampilleta, S. Klyatskaya, J.-P. Cleuziou, M. Ruben and W. Wernsdorfer, *Nat. Mater.*, 2011, **10**, 502–506.
64 A. Hauser, *Coord. Chem. Rev.*, 1991, **111**, 275–290.
65 I. Šalitroš, O. Fuhr, R. Kruk, J. Pavlik, L. Pogány, B. Schäfer, M. Tatarko, R. Boča, W. Linert and M. Ruben, *Eur. J. Inorg. Chem.*, 2013, **2013**, 1049–1057.
66 E. W. Mueller, J. Ensling, H. Spiering and P. Guetlich, *Inorg. Chem.*, 1983, **22**, 2074–2078.
67 C. N. R. Rao, H. S. S. Ramakrishna Matte, K. S. Subrahmanyam and U. Maitra, *Chem. Sci.*, 2012, **3**, 45–52.

